Downloaded from orbit.dtu.dk on: Apr 19, 2024

DTU Library

Wafer-Scale Polymer-Based Transparent Nanocorals with Excellent Nanoplasmonic Photothermal Stability for High-Power and Superfast SERS Imaging

Wu, Kaiyu; Nguyen, Long Quang; Rindzevicius, Tomas; Keller, Stephan Sylvest; Boisen, Anja

Published in:
Advanced Optical Materials

Link to article, DOI:
10.1002/adom.201901413

Publication date:
2019

Document Version
Peer reviewed version

Link back to DTU Orbit

Citation (APA):
Wu, K., Nguyen, L. Q., Rindzevicius, T., Keller, S. S., & Boisen, A. (2019). Wafer-Scale Polymer-Based Transparent Nanocorals with Excellent Nanoplasmonic Photothermal Stability for High-Power and Superfast SERS Imaging. *Advanced Optical Materials*, *7*(23), Article 1901413. https://doi.org/10.1002/adom.201901413

General rights
Copyright and moral rights for the publications made accessible in the public portal are retained by the authors and/or other copyright owners and it is a condition of accessing publications that users recognise and abide by the legal requirements associated with these rights.

- Users may download and print one copy of any publication from the public portal for the purpose of private study or research.
- You may not further distribute the material or use it for any profit-making activity or commercial gain
- You may freely distribute the URL identifying the publication in the public portal

If you believe that this document breaches copyright please contact us providing details, and we will remove access to the work immediately and investigate your claim.

Wafer-scale Polymer-based Transparent Nanocorals with Excellent Nanoplasmonic Photothermal Stability for High-power and Superfast SERS Imaging

Kaiyu Wu, Long Quang Nguyen*,Tomas Rindzevicius, Stephan Sylvest Keller and Anja Boisen*

Dr. K. Wu, Assoc. Prof. T. Rindzevicius, Prof. A. Boisen
Department of Health Technology, DTU Health Tech, Technical University of Denmark, 2800, Kgs. Lyngby, Denmark

Dr. L. Q. Nguyen, Assoc. Prof. S. S. Keller
National Center for Nano Fabrication and Characterization, DTU Nanolab, Technical University of Denmark, 2800, Kgs. Lyngby, Denmark

Dr. K. Wu, Dr. L. Q. Nguyen, Assoc. Prof. T. Rindzevicius, Assoc. Prof. S. S. Keller, Prof. A. Boisen
DNRF and Villum Fonden Center for Intelligent Drug Delivery and Sensing Using Microcontainers and Nanomechanics, IDUN, Technical University of Denmark, 2800, Kgs. Lyngby, Denmark

E-mail: kaiwu@dtu.dk, longq@dtu.dk

Keywords: surface-enhanced Raman spectroscopy, nanoplasmonic heating, large-area, SERS substrate, uniform

Polymer-based SERS substrates offer distinctive advantages such as low-cost and high optical transparency which allows direct detection of trace chemicals on target surfaces and easy microfluidic integration. However, incident laser-induced localized surface plasmon resonances can generate heat that deform the polymer and significantly reduce the intensities of recorded SERS signals. Herein, a novel wafer-scale polymer-based transparent nanocoral (WTNC) SERS substrate with 3D electromagnetic “hotspots” is presented. Its fabrication is simple and lithography-free. The novel SERS substrate demonstrates excellent nanoplasmonic heat resistance, high SERS sensitivity, and unmatched SERS signal uniformity with a relative standard deviation of ~ 6% across 80 mm. Excellent photothermal stability is achieved by highly crosslinking SU-8, a negative epoxy photoresist, raising its initial degradation temperature to ~230 °C, much higher than the glass transition temperature of state-of-the-art thermalplasts used in SERS substrates, including PET and PMMA. The WTNC substrate can withstand very high laser irradiance of up to 300 kW cm^{-2}, enabling superfast SERS imaging

of analytes in extremely small quantities. A high resolution SERS image containing 10201 spectra of ~44 attomol trans-1,2-bis(4-pyridyl)ethylene is obtainable in < 5 minutes. The WTNC substrate pushes the state-of-the-art in polymer-based SERS substrates and has great potential for rapid routine analyses.

1. Introduction

Surface-enhanced Raman spectroscopy (SERS) is an ultrasensitive analytical technique.[1-3] It probes the tremendously enhanced Raman spectral fingerprints of molecules in plasmonic hotspots e.g., in nanogaps and near tips of metallic nanostructures.[4-6] Even a single molecule can be detected if SERS enhancement factor (EF) reaches ~10^8 – 10^9.[7] Refinement of plasmonic nanomaterials,[8-10] advancement in laser systems,[11,12] and development of efficient sample pre-treatment methods,[13-15] have jointly pushed the utility of SERS into various fields, ranging from biosensing[16,17] and environmental monitoring,[18-20] to anti-counterfeiting applications[21-23] and fundamental research.[24-26]

The success of SERS is highly dependent on the development of plasmonic nanomaterials that amplify the Raman scattering signal. Modern SERS substrates i) are compatible with large-scale manufacturing processes, ii) have acceptable batch-to-batch SERS signal intensity variations, and iii) exhibit high and reproducible EFs over large surface areas.[27-31] In addition, the most competitive SERS substrates offer new, important functionalities, e.g. reusability,[32] transparency and softness,[33,34] concentration of analytes in electromagnetic (EM) hotspots,[35] or enhancement of the Raman signal using nanogap-free structures,[36] which further facilitates the development of SERS applications at low-cost.

Recently, polymer-based SERS substrates have attracted immense attention due to their distinctive advantages, e.g. i) cheap production using large-scale and high-throughput fabrication processes, such as injection molding and screen printing,[37,38] ii) easy integration with microfluidics platforms allowing elaborated, on-chip sample pre-treatments which are

important for sensing applications,[39,40] iii) optical transparency, which enables SERS signals to be probed from the backside of the substrate. This property is extremely useful for direct detection of trace chemicals on target surfaces, e.g. ractopamine (feed additive) residue on pork[41], malachite green (highly toxic) on fish,[42] Raman imaging of molecules using SERS-active metafilms.[43] iv) Integration of disposable substrates on curved surfaces, which further increase practical uses of polymer-based SERS substrates.[44]

Despite the numerous advantages of polymer-based SERS substrates, their practical applicability is strongly restricted by their generally poor heat resistance, which, to the best of our knowledge, has never been addressed. Incident laser-induced surface plasmon resonances can cause enormous local heating, which deform the polymer and dramatically reduce SERS signal intensity. Specifically, during SERS measurements, the temperature on the surface of SERS substrates could reach >140 °C[45] in tens of seconds[46], exceeding glass transition temperatures (T_g) of most commonly used polymers for SERS substrates, e.g., polyethylene terephthalate, i.e. PET (T_g = 67 °C),[47] TOPAS (T_g = 134 °C),[48] Poly(methyl methacrylate), i.e. PMMA (T_g = 105 °C),[49] and polystyrene ($T_g \approx$ 100 °C).[50] Since the intensity of probed SERS signals (I_{SERS}) is proportional to the intensity of excitation laser (I_L) and the time of collection (t), the issue could be temporarily solved by lowering I_L while extending t. This would however, considerably increase the time of SERS imaging. In SERS mapping, which is often required for reliable and quantitative analyses of trace analytes[51,52] and where typically thousands of spectra are recorded, this would result in several hours of data collection.

To facilitate wide use of SERS for routine analyses and push the state-of-the-art of SERS substrates, there is a need to develop a polymer-based SERS substrate, which exhibits high nanoplasmonic photothermal stability, as well as other properties of modern polymer-based SERS substrates as described above. From a practical point of view, its success would allow superfast, large-area SERS imaging with high resolution, high sensitivity and high reliability, greatly facilitating practical use of polymer-based SERS substrates. Here, we propose a

solution, based on wafer-scale, non-lithographic nanostructuring of highly cross-linked negative epoxy photoresist SU-8. The key lies in the completion of the cross-linking process, after which initial degradation temperature of SU-8 increases to ~230 °C,[53] which is much higher than that of partially cross-linked SU-8[53] and the glass transition temperature of state-of-the-art thermalplasts used in SERS substrates.[47-50] In addition, nanostructuring of partially cross-linked SU-8 has been realized by maskless reactive ion etching (RIE),[54,55] which is simple, fast, reproducible, and suitable for large-format production in standard IC foundries. The process is inspiring for development of new SERS-active materials using highly cross-linked SU-8 polymers through systematic hot spot engineering.

In this work, we report a novel wafer-scale, polymer-based transparent nanocoral (WTNC) SERS substrate with 3D hotspots demonstrating excellent nanoplasmonic heat resistance, ultrahigh sensitivity, and unmatched SERS signal uniformity, suitable for reproducible, high-power and superfast SERS imaging of trace analytes. Its fabrication process is very simple. The WTNC substrate is manufactured via maskless RIE on a polished 4-inch fused silica wafer covered by a highly cross-linked SU-8 layer, followed by e-beam evaporation of gold. Particularly, the developed RIE process induces minimal macro-loading effect, and therefore renders uniform structures across the wafer, even near its edge, resulting in supreme SERS signal uniformity with a relative standard deviation (RSD) of ~ 6% across 80 mm on a 4-inch wafer. In addition, through systematic hotspot engineering, SERS EF is maximized for 780 nm excitation, facilitating the use of the substrate for biological and medical applications. Besides high sensitivity, the WTNC substrate demonstrates excellent nanoplasmonic photothermal stability. It can withstand very high laser intensity of up to 300 kW cm^{-2}. SERS spectrum of ~44 attomol trans-1,2-bis(4-pyridyl) ethylene (BPE) is obtainable, using very high excitation intensity of 50 kW cm^{-2}, with extremely short collection time of 25 ms. It is particularly impressive that obtaining a high resolution SERS image containing 10201 of these spectra, requires less than 5 minutes. Moreover, the WTNC substrate exhibits high

optical transparency. SERS intensity decreases only by half when probed from its backside. Furthermore, the use of SU-8 allows potential integration of the SERS substrate with microfluidics, via simple and rapid processes such as ultrasonic wielding, facilitating even wider laboratorial and mobile applications in practice.

2. Results and Discussion

2.1. Fabrication of the WTNC SERS Substrate

The fabrication process of the WTNC SERS substrate is illustrated in **Figure 1**a-c. The entire process is performed using standard silicon processing equipment available in the semiconductor industry, and can therefore be conducted in most research institutions and IC foundries.

The process contains three steps. Firstly, SU-8 photoresist is spin coated onto a 4-inch fused silica wafer, covering the entire surface. Fused silica is used due to its well-known excellent optical transparency in the visible to NIR range. Then, the SU-8 coating is highly cross-linked via UV exposure with a dose of 1 J cm^{-2} and hard baking at 250 °C for 20 min. The step should allow the produced nanocoral SERS substrate to be used in high-power and superfast SERS imaging during which structural deformation can occur to most polymer-based SERS substrates due to local nanoplasmonic heating. This is because during crosslinking of SU-8, the epoxy groups of the monomers react within the ones of a different monomer. By a high degree of crosslinking, a much denser polymer network is produced. Given that SU-8 is a thermoset resin, eventual heating induced by plasmonic interactions only further promotes crosslinking and results in a highly stable polymer network. For thermal decomposition, temperatures of above 300 °C have to be reached.[56] Secondly, maskless RIE using O_2 plasma is carried out to nanostructure the SU-8 layer, rendering flexible SU-8 nanostructures uniformly over the whole wafer. During the RIE, the antimony being an intrinsic component of the SU-8 crosslinking agent is not removed but gradually accumulates

at the surface of the etched substrates. The antimony then serves as local etching mask (micro-masking effects), and provides starting points for fabrication of the nanowires. Finally, to render the substrate SERS-active, deposition of gold is performed by e-beam evaporation after O_2 RIE. Gold is chosen due to its stability which extends shelf life of the WTNC SERS substrates. During gold deposition, a shadow mask with a specific pattern can be employed on the wafer to render bare SU-8 areas, facilitating further processes to be performed, such as laser dicing and microfluidic integration by ultrasonic wielding.[39,57] A photograph of a WTNC SERS substrate taken from its backside is shown in Figure 1f.

The nanocorals are visualized using SEM, shown in Figure 1d and 1e, from cross-sectional and vertical view, respectively. These images reveal that the nanocorals are clusters of curved SU-8 nanowires covered by gold with a rough surface. This suggests that under excitation, 3D EM hotspots with enhanced electrical fields[60] can be developed in i) the nanogaps between the gold covered nanowires, ii) the nanogaps between the gold covered nanowires and the underlying gold film, and iii) the nanotrenches on the gold surface of the nanowires.

Note that the use of pure O_2 plasma is advantageous.[58] Maskless RIE using mixed SF_6 and O_2 plasma is frequently employed to produce other state-of-the-art wafer-scale SERS substrates, such as the widely used metal-capped silicon nanopillars.[27,59] It, however, usually causes significant structural inhomogeneity across the wafer, due to pronounced macro-loading effect, leading to poor yield and non-uniform SERS signals.[59] Macro-loading effect means that etch rate becomes slower with more exposed etch area, due to depletion of etchant. For maskless RIE using a barrel etcher, more etchant is depleted towards the center of the wafer. Therefore, the etch rate becomes slower towards the center of the wafer, resulting in center-to-edge uniformity issues, e.g., bull's eye effect. In the maskless RIE process fabricating WTNC SERS substrates, very high coil power (2000 W) and etchant flux (99 sccm of O_2) are employed. This helps maintain sufficient etchant supply, thus minimizes macro-loading effect. **Figure 2** shows comparison of a WTNC SERS substrate fabricated by

maskless O_2 RIE followed by gold metallization, and a gold capped silicon nanopillar substrate fabricated using maskless O_2 + SF_6 RIE (both in 4-inch). The uniform plasmonic structural color of the WTNC substrate indicates uniform distribution of the nanostructures over the entire wafer.

The use of highly cross-linked SU-8 is beneficial for realizing high optical transparency of the WTNC SERS substrate. This can be attributed to the very high optical transparency of highly cross-linked SU-8 (transmittance > 95%) near the SERS excitation wavelength (780 nm).[61] Figure 1g shows that the SERS signal, obtained on a WTNC SERS substrate produced with optimal process parameters, drops by only about half when probed from its backside.

2.2. Uniform Hot Spot Engineering of the WTNC SERS Substrate

2.2.1. Experimental Maximization of SERS Sensitivity

High sensitivity is a prerequisite for a SERS substrate to be used for efficient SERS analyses. Here, the maximization of SERS sensitivity under a 780 nm excitation is demonstrated for the WTNC substrate. 780 nm is chosen because i) cross-linked SU-8 exhibits excellent optical transparency at 780 nm,[61] ii) 780 nm is in the biological window, therefore maximized SERS sensitivity at 780 nm will facilitate the use of the WTNC substrate for wider biological and medical applications, and iii) solid-state 780 nm or 785 nm lasers are accessible in most laboratory and handheld Raman spectrometers. The optimization of the sensitivity is systematically done by i) varying the density of the nanocorals, ii) changing the height of the nanocorals by changing the duration of the RIE process (t_{RIE}), and iii) altering the thickness of the deposited gold (D_{au}).

For a SERS substrate, increasing the density of the nanostructures is usually advantageous. This is because with a higher structural density, the laser spot covers a greater number of EM hotspots, leading to stronger and more uniform SERS signals. It is found that the type of the employed SU-8 affects the density of the produced nanostructures, as is shown in **Figure S1**b

in the supporting information. As a result, highest SERS intensity is achieved on the WTNC substrate with the highest density of nanocorals, obtained using SU-8 2035 (Figure S1a). Therefore, SU-8 2035 is chosen for the rest of the optimization process. The change in density is due to the different concentration of antimony in different types of SU-8.[58]

The RIE process time t_{RIE} has a major influence on the height of the nanocoral structures, and thus on the SERS intensity I_{SERS}. **Figure 3**a shows that maximum I_{SERS} is achieved when t_{RIE} = 120 s. It also shows that increasing t_{RIE} from 60 - 120 s leads to ~5 times stronger I_{SERS}, and I_{SERS} decreases by ~10 times when further increasing t_{RIE} from 120 - 540 s. To assess the cause of the sharp maxima of I_{SERS} at t_{RIE} = 120 s, SEM imaging was performed for the nanocoral substrates processed with t_{RIE} varing from 60 - 420 s, as shown in Figure 3b. It can be seen that longer t_{RIE} results in taller nanocorals. In addition, since taller SU-8 nanowires are flexible, longer t_{RIE} also renders nanocorals of larger sizes. The increase in I_{SERS} when extending t_{RIE} from 60 - 120 s can be ascribed to the formation of more nanogap junctions between gold surfaces in the nanocorals. Further increasing t_{RIE}, however, decreases the plasmonic coupling strength between the nanocorals and the underlying gold film. This should result in weaker EM enhancement and thus weaker I_{SERS}.

Using the optimal t_{RIE} = 120 s, D_{au} is varied between 160 - 300 nm, to further maximize SERS sensitivity for the WTNC substrates. The results are shown in Figure 3c. It can be seen that the highest I_{SERS} is achieved when D_{au} = 240 nm. This could be attributed to the highest proximity, i.e., strongest coupling, between the bottom of the gold covered nanocorals and the underlying gold film, indicated by the SEM images shown in Figure 3d. Moreover, Figure 3d shows that when D_{au} = 300 nm, part of the gold is fused and continuous gold layers are formed. This decreases the number of nanogap-based EM hotspots, resulting in weaker I_{SERS}.

In summary, to achieve optimal SERS sensitivity on the WTNC substrates under a 780 nm excitation, SU-8 type 2035, t_{RIE} = 120 s and D_{au} = 240 nm should be employed.

2.2.2. Clustering of Nanocorals

Since the SU-8 structures are flexible, lateral capillary forces can pull adjacent nanocoral clusters together during the evaporation of analyte solution on the nanocoral surface. This creates larger nanocoral clusters containing more nanogaps, i.e., EM hotspots, and potentially leads to higher SERS sensitivity. To evaluate this effect, the following experiment is performed. Thiophenol is first evaporated onto WTNC substrates with structures of different heights, processed with t_{RIE} = 60, 120, and 300 s. Afterwards, a droplet of deionized water is deposited onto each substrate. SERS measurements are carried out before and after deposition and drying of the deionized water. The results are shown in **Figure 4**a. It can be seen that I_{SERS} i) remains almost identical for the substrate with short nanocorals produced with t_{RIE} = 60 s, and ii) increases by ~3 times for substrates covered by taller nanocoral structures produced with t_{RIE} = 120 and 300 s upon water deposition. Top-view SEM images of these substrates are taken before and after deposition and evaporation of deionized water to assess the cause of this, and are shown in Figure 4b. The SEM images confirm that the increase of I_{SERS} observed in Figure 4a is caused by clustering of the nanocoral clusters, after which additional nanogaps, i.e., EM hotspots, are created in the nanostructures. These results show that when using the WTNC substrates for sensing analytes in gas phase, solvent should be deposited onto the substrate after introducing the analytes to obtain a maximized number of EM hotspots and the strongest SERS signals.

2.2.3. Optical Properties of the WTNC SERS Substrates

The far-field optical response of the WTNC SERS substrates is shown in **Figure 5**a, as dark-field scattering spectra. They reveal that i) for all the WTNC substrates, the scattering maxima is near 800 nm. ii) Increasing t_{RIE} from 60 to 540 s redshifts the scattering peak from ~ 770 to ~850 nm. Referring to the SEM images in Figure 3b, this red shift can be ascribed to the collective effect of the stronger plasmonic couplings in larger clusters.[62] iii) clustering of nanocorals during evaporation of solvent has negligible effect on the scattering peak position. This could be ascribed to the small number of newly formed nanogap junctions upon

clustering of nanocorals, indicated by Figure 4a, showing that I_{SERS} increases only ~3 times after clustering of nanocorals. iv) For a WTNC substrate fabricated with optimal t_{RIE} = 120 s, the scattering peak position is not sensitive to D_{au}, i.e., not sensitive to the change in morphology of gold. A total redshift of ~ 30 nm from ~785 to ~815 nm is observed when increasing D_{au} from 160 to 300 nm. Such a small redshift can be attributed to the increase in the average size of the gold clusters.

To estimate the maximum SERS EF and determine the locations of hotspots for the WTNC substrate, numerical simulations are performed. The simulated structures are modelled referring to cross-sectional SEM images of the nanocorals fabricated using optimal parameters (SU-8 2035, t_{RIE} = 120 s and D_{au} = 240 nm) such as the one shown in Figure 3d. The modelled structures are significantly simplified to be computable. Ellipsoids are used to approximate gold covering the SU-8 nanowires, which are represented by cylinders. Such simplification is reasonable, since the optical property of the nanocorals is not sensitive to the change in the morphology of gold on their top, as has been shown previously by the dark-field scattering spectra. The calculated electrical field EF distributions, i.e., E/E_0, where E_0 represents the magnitude of the excitation field, are plotted in Figure 5b. The field distribution reveals that EM hotspots of the WTNC SERS substrates are located in the gap junctions between i) the gold covered SU-8 nanowires, and ii) the gold covered nanowires and the underlying gold film. In this context it should be noted that 3D hotspots are an advantage of the nanocoral SERS substrate. These 3D hotspots enhance Raman scattering signals of analytes both near the underlying gold film and in the vicinity of the suspended nanogap junctions. This is particularly correct when the substrate is hydrophilic. In this case, the analyte solution spreads over a large surface area. Due to fast solvent evaporation, more analytes will adsorb on the underlying gold film.[63] In addition, the simulation shows a maximum electrical field EF > 1000, with a minimum gap distance between gold being 1.5

nm. According to the well-known E^4 approximation, this leads to a maximum theoretical SERS EF > 1.0×10^{12}.

The surface-average SERS EF is also important in practice, since in most cases a significant number of analytes are deposited or immobolized outside of EM hot spots. The surface-average SERS EF of the WTNC substrate is estimated by assuming that all the probed analytes, regardless of their location on the substrate, contribute equally to the SERS signal. The following equation is used for the estimation:

$$\overline{EF} = \frac{I_{SERS}/N_{TOTAL}}{I_{RS}/N_{RS}} \quad (1)$$

where I_{SERS} and I_{RS} are the SERS and the Raman intensity, respectively. N_{TOTAL} is the total number of molecules probed by the laser in the SERS measurement. Note that N_{TOTAL} is not the number of molecules located inside or near the hot spots, which is a dramatically lower number, often used to estimate average SERS EFs. N_{RS} is the number of molecules probed in the Raman measurement. To obtain I_{RS} and N_{RS}, a 0.1 M ethanol solution of BPE is poured into a petri dish. 0.9 counts mW^{-1} s^{-1} are observed under a 780 nm excitation. Using the interaction volume of 60 um^3, N_{RS} is ~4×10^9. To obtain I_{SERS} and N_{TOTAL}, 1 nanomol BPE in ethanol is deposited onto the WTNC SERS substrate. The droplet spreads over the substrate surface and dries within several seconds. The introduced solution forms a quasi-circular pattern on the surface of the substrate, with a radius of ≈ 4500 μm. This leads to an average density of BPE on the substrate being ~ 9.5×10^6 μm^{-2}. Using identical conditions as for I_{RS}, I_{SERS} ≈ 6100 mW^{-1} s^{-1} is measured for the 1200 cm^{-1} BPE peak. With a laser spot size of 0.94 μm in radius, N_{TOTAL} is 2.6×10^7 (~44 attomol). Hence, the calculated surface-averaged SERS EF is 1×10^6 for the WTNC substrate.

2.3. Nanoplasmonic Photothermal Stability of the WTNC SERS Substrate

Firstly, the maximum SERS laser intensity that does not lead to structural changes of the WTNC substrate has to be identified. For this purpose, arrays of square areas (100 × 100 $\mu m^{2)}$ are scanned with increasing laser intensities (I_{SC}). Afterwards, 1 nanomol BPE in 1 μL ethanol

solution is pipetted onto the substrate. Following the drying of the substrate, a SERS image is obtained over the entire substrate surface. It is important to note that the laser scans are performed before introducing the analytes. This is to eliminate the effect of decomposition and desorption of analyte molecules on the SERS signals under extremely high excitation laser intensities. A representative SERS image is shown in **Figure 6**a. It can be seen that by applying I_{SC} > 50 kW cm^{-2}, I_{SERS} decreases, suggesting structural changes of the nanocoral substrate. Such structural changes are also indicated by the plasmonic color changes shown in Figure 6b, where a microscopic image corresponding to the SERS imaged area in Figure 6a is shown. For quantitative analysis, Figure 6c plots the relative I_{SERS} of BPE at 1200 cm^{-1} versus I_{SC}. It can be seen that the SERS performance of the nanocoral substrate degrades when I_{SC} > 50 kW cm^{-2}, and the substrate becomes SERS-inactive when I_{SC} reaches 400 kW cm^{-2}. Interestingly, the decrease of I_{SERS} appears to be a 2-step process. The first major decrease that occurs when increasing I_{SC} from 50 – 100 kW cm^{-2} is probably due to deformation of the nanocoral structures when the SU-8 softens. The second major decrease happens when I_{SC} reaches 350 kW cm^{-2}. This is caused by thermal decomposition of SU-8, i.e., pyrolysis, which is revealed by the Raman spectra shown in Figure 6d, where the D- and G- bands of carbon appear and the main SU-8 peak at ~640 cm^{-1} vanishes.

To summarize, the WTNC SERS substrate maintains its full SERS performance for laser intensities ≤ 50 kW cm^{-2}, and is capable of withstanding extremely high laser intensity of up to 300 kW cm^{-2}, at the cost of decreasing the signal intensity to half the value.

To further demonstrate the thermal stability of the WTNC substrate, its performance is compared with a transparent TOPAS-based (T_g of TOPAS = 134 °C)[48] SERS substrate with similar surface-averaged SERS EF of ~ 1 × 10^6.[39] Before introducing BPE analytes onto the substrates, a laser scan is performed on the WTNC and the TOPAS-based substrate in the dotted areas shown in **Figure S2**a-b with I_{SC} = 50 and 15 kW cm^{-2}, respectively. Afterwards, 1 nanomol BPE in 1 μL ethanol solution is pipetted onto each substrate. SERS images in

Figure S2 are then obtained after drying of the substrates, using a 780 nm laser at 50 and 10 kW cm^{-2}, for the WTNC and TOPAS substrate, respectively. 10 kW cm^{-2} is used since for a laser intensity > 10 kW cm^{-2} the SERS performance of the TOPAS substrate degrades, as indicated in Figure S2. The SERS images in Figure S2 show that the WTNC substrate can operate at roughly 5 times higher laser intensity without losing SERS signals, compared with the TOPAS-based substrate.

2.4. SERS Uniformity of the WTNC Substrate

High SERS signal uniformity is mandatory for achieving reliable and quantitative SERS analysis. **Figure 7**a shows that the WTNC substrate exhibits superb SERS uniformity across 80 mm with RSD of ~6%. Such uniformity, to the best of our knowledge, is unmatched, resulting from i) the extremely dense 3D hot spots of the nanocoral structures, and ii) the employment of a wafer-scale maskless O_2 RIE process with minimized macroloading effect.

Due to the collective effect of i) the electrical field in EM hot spots being inhomogeneous in nature and very sensitive to the detailed shape of the plasmonic nanostructures,[64] and ii) the uneven distribution of analytes in individual hot spots, it is also necessary to evaluate SERS uniformity with analytes of extremely low quantities. To perform such a measurement, 1 nanomol BPE in 1 μL ethanol solution is deposited onto the WTNC substrate. The droplet spreads and wets the surface quasi-circularly (~4.5 mm in radius). After drying, the entire droplet area is imaged by SERS, and the result is shown in Figure 7b. The symmetry of the SERS image towards the center of the droplet indicates that the WTNC substrate is capable of reproducing SERS spectra of extremely low concentrated analytes. Assuming uniform adsorption of BPE onto the substrate, and taking into account that the radius of the laser spot is 0.94 μm, ~44 attomol BPE in average is contributing to each SERS spectrum. To further quantify the SERS uniformity, SERS imaging is carried out over a 1000 × 1000 μm^2 square near the center of the droplet in Figure 7b, using a step size of 10 μm. The results are shown in Figure 7c, where a RSD of ~11% is obtained. In addition, Figure 7c shows that with 50 kW

cm^{-2} laser intensity and 25 ms exposure time, an uniform SERS signal from ~44 attomol BPE is obtainable, and the total collection time for the high-resolution SERS image containing 10201 points is < 5 min. These results demonstrate that the WTNC substrate is capable of enhancing Raman spectra for analytes of extremely small quantities to a detectable level in a reproducible and reliable manner with high-power and superfast SERS imaging.

3. Conclusion

We have designed and fabricated a unique transparent polymer-based WTNC SERS substrate with 3D hotspots demonstrating excellent nanoplasmonic heat resistance, ultrahigh SERS sensitivity, and supreme SERS signal uniformity. The high thermal stability allows high-power and superfast SERS imaging for analytes of extremely small quantity with excellent reliability and signal reproducibility. Its fabrication is simple, lithography-free, wafer-scale, and can be conducted in any research institution with standard silicon processing equipment. Particularly, high nanoplasmonic photothermal stability is realized by crosslinking SU-8 to a very high degree. The employed RIE process induces minimal macro-loading effect, and renders uniform nanostructures across the wafer, resulting in unrivalled SERS signal uniformity with a RSD of ~ 6% across 80 mm on a 4-inch substrate. By systematic hotspot engineering, SERS sensitivity is maximized in the biological window at 780 nm excitation. The estimated maximum and surface-averaged SERS EF is 1.0×10^{12} and 1×10^{6}, respectively. SERS spectrum of ~44 attomol BPE is obtainable under very high excitation intensity of 50 kW cm^{-2} with an extremely short collection time of 25 ms. Obtaining a high resolution SERS image containing 10201 of these spectra requires < 5 minutes. In addition, the WTNC SERS substrate can withstand extremely high laser intensity of up to 300 kW cm^{-2}, at the cost of about half of the SERS signal intensity. Furthermore, the substrate is highly transparent. SERS intensity decreases only by half when probed from the backside. The excellent SERS performance and the high nanoplasmonic photothermal stability, paired with

the simple fabrication, allow the WTNC SERS substrates to be used in a large number of laboratory and mobile applications. The design of the substrate also opens up for its integration with microfluidic systems facilitating on-chip, elaborated sample pre-treatments that are often required for practical applications.

4. Experimental Section

Fabrication of the WTNC SERS Substrates: SU-8 photoresist type 2005, 2035, or 2075 was spin coated on a 4-inch double-side polished fused silica wafer at 2000 rpm for 30 seconds using a Süss MicroTec RCD8 T spin coater. After solvent evaporation at room temperature, flood UV exposure was performed on a Süss MicroTec MA6/BA6 aligner with a dose of 1 J cm^{-2} at the I-line. The samples were subsequently baked for 1 hour at 50 °C on a hotplate followed by 20 minutes hard baking at 250 °C in an oven. Maskless RIE was then performed in an STS MESC Multiplex ICP Advanced Silicon Etcher using 2000 W coil power, 30 W platen power, 99 sccm of O_2, and a 20 mTorr chamber pressure at 20 °C. Subsequent e-beam evaporation of gold was conducted in Wordentec QCL 800 under 4×10^{-6} mbar with a deposition rate of 10 Å s^{-1}.

SEM Characterizations: SEM images were taken in a Zeiss Ultra Plus field emission scanning electron microscope equipped with a Gemini column. The accelerating voltage was 4 kV. The cross-sectional images were taken at a tilted angle of 5° (45° for the images in Figure 3b). No additional coating was applied to the samples.

SERS measurements: A Thermo Scientific DXRxi confocal Raman microscope was used. Unless otherwise noted, a 780 nm excitation laser was used at 50 kW cm^{-2} with 25 ms time of collection. Unless otherwise noted, a 10× objective (spot size: 1.87 μm in radius) and a 50× objective (spot size: 0.94 μm in radius) was used for laser intensity ≤ 200 kW cm^{-2} and > 200 kW cm^{-2}, respectively. For SERS images in Figures 6 and Figure S2, the 50× objective was used. The microscope was coupled to a single-grating spectrometer with a 5 cm^{-1} full width at

half maximum spectral resolution and a ±2 wavenumber accuracy. A 50 μm slit was used. All SERS measurements were conducted at room temperature.

Dark-field Scattering Measurements: A Nikon Ti-U inverted microscope equipped with a CF LU Plan Fluor Epi 50× objective was used. The objective had a NA of 0.8 and working distance of 1 mm. The angle of incidence was ~50°. Scattered light was collected from the front side of the samples, i.e., surfaces topped by nanostructures, through the center of the objective, and was subsequently guided into a spectrometer (Shamrock Spectrograph SR-303IA equipped with an Andor Newton 970 EMCCD). The obtained spectrum was then divided by the reference white light spectrum to reveal the scattering signal from the samples.

Numerical Simulations: FEM simulations were carried out using COMSOL MULTIPHYSICS version 4.4. To achieve reasonable computation time, ellipsoids were used to approximate gold. SU-8 structures were modelled by cylinders. The linearly polarized excitation wave with a wavelength of 780 nm was generated on a domain-backed port, placed at the top of the solution domain. A perfect matched layer was employed linking to the top and bottom planes of the solution domain to eliminate nonphysical reflection. The boundary conditions for the side planes were Floquet periodicity. Materials were modeled by their complex refractive indices as functions of wavelength.[65, 66] The medium surrounding the nanostructures was vacuum. The EM field distribution was obtained by solving the full field.

Supporting Information

Supporting Information is available from the Wiley Online Library or from the author.

Acknowledgements

The authors would like to thank Marlitt Viehrig for providing the TOPAS substrate, Jesper Scheel for the beautiful photographs, Dr. Onur Durucan, Dr Oleksii Ilchenko, Dr Lasse Højlund Eklund Thamdrup and Senior Researcher Michael Stenbæk Schmidt for their advice and comments. This work was supported by the Danish National Research Foundation (Project DNRF122) and Villum Fonden (Grant No. 9301).

Received: ((will be filled in by the editorial staff))
Revised: ((will be filled in by the editorial staff))
Published online: ((will be filled in by the editorial staff))

References

[1] M. G. Albrecht, J. A. Creighton, *J. Am. Chem. Soc*., **1977**, *99*, 5215.

[2] D. L. Jeanmarie, R. P. Van Duyne, *J. Electroanal. Chem*., **1977**, *84*, 120.

[3] M. Fleischmann, P. J. Hendra, A. J. McQuillan, *Chem. Phys. Lett*., **1974**, *26*, 163.

[4] H. Xu, J. Aizpurua, M. Käll, and P. Apell, *Phys. Rev. E*, **2000**, *62*, 4318.

[5] D.-K. Lim, K.-S. Jeon, H. M. Kim, J.-M. Nam, Y. D. Suh, *Nat. Mater*., **2010**, *9*, 60.

[6] D. Jimenez de Aberasturi, A. B. Serrano-Montes, J. Langer, M. Henriksen-Lacey, W. J. Parak, L. M. Liz-Marzan, *Chem. Mater*., **2016**, *28*, 6779.

[7] E. C. Le Ru, P. G. Etchegoin, *Annu. Rev. Phys. Chem*., **2012**, *63*, 65.

[8] S.-Y. Ding, J. Yi, J.-F. Li, B. Ren, D.-Y. Wu, R. Panneerselvam, Z.-Q. Tian, *Nat. Rev. Mater.* **2016**, *1*, 16021.

[9] S. Schlücker, *Angew. Chem. Int. Ed*. **2014**, *53*, 4756.

[10] C. Hanske, M. N. Sanz-Ortiz, L. M. Liz-Marzán, *Adv. Mater*., **2018**, *30*, 1707003.

[11] F. Ariese, H. Meuzelaar, M.M. Kerssens, J.B. Buijs, C.Gooijer, *Analyst*, **2009**, *134*, 1192.

[12] J. Zhao, K. A. Bakeev, J. Zhou, *Photonics Spectra*, **2018**, *52*, 44.

[13] S. Pal, S. Harmsen, A. Oseledchyk, H.-T. Hsu, .M. F. Kircher, *Adv. Funct. Mater.*, **2017**, *27*, 1606632.

[14] O. Durucan, T. Rindzevicius, M. S. Schmidt, M. Matteucci, A. Boisen, *ACS Sens.*, **2017**, *2*, 1400.

[15] I. J. Jahn, O. Žukovskaja, X.-S. Zheng, K. Weber, T. W. Bocklitz, D. Cialla-May, J. Popp, *Analyst*, **2017**, *142*, 1022.

[16] C. Zong, M. Xu, L. J. Xu, T. Wei, X. Ma, X. S. Zheng, R. Hu, B. Ren, *Chem. Rev.*, **2018**, *118*, 4946.

[17] S. Laing, L. E. Jamieson, K. Faulds, D. Graham, *Nat. Rev. Chem.*, **2017**, *1*, 0060.

[18] A. Hakonen, P. O. Andersson, M. S. Schmidt, T. Rindzevicius, M. Käll, *Analytica Chimica Acta*, **2015**, *893*, 1.

[19] S. Bai, D. Serien, A. Hu, K. Sugioka, *Adv. Funct. Mater.*, **2018**, *28*, 1706262.

[20] R. A. Halvorson, P. J. Vikesland, *Environ. Sci. Technol.*, **2010**, *44*, 7749.

[21] Y. Liu, Y. H. Lee, M. R. Lee, Y. Yang, X. Y. Ling, *ACS Photonics*, **2017**, *4*, 2529.

[22] D. Li, L. Tang, J. Wang, X. Liu, Y. Ying, *Adv. Opt. Mater.*, **2016**, *4*, 1475.

[23] K. J. Si, D. Sikdar, L. W. Yap, J. K. K. Foo, P. Guo, Q. Shi, M. Premaratne, W. Cheng, *Adv. Opt. Mater.*, **2015**, *3*, 1710.

[24] W. Xie, B. Walkenfort, S. Schlücker, *J. Am. Chem. Soc.*, **2013**, *135*, 1657.

[25] B. Sharma, R. R. Frontiera, A. I. Henry, E. Ringe, R. P. Van Duyne, *Mater. Today*, **2012**, *15*, 1.

[26] E. A. Sprague-Klein, B. Negru, L. R. Madison, S. C. Coste, B. K. Rugg, A. M. Felts, M. O. McAnally, M. Banik, V. A. Apkarian, M. R. Wasielewski, M. A. Ratner, T. Seideman, G. C. Schatz, R. P. Van Duyne, *J. Am. Chem. Soc.*, **2018**, *140*, 10583.

[27] M. S. Schmidt, J. Hübner, A. Boisen, *Adv. Mater.*, **2012**, *24*, OP11.

[28] K. N. Kanipe, P. P. F. Chidester, G. D. Stucky, M. Moskovits, *ACS Nano*, **2016**, *10*, 7566.

[29] N. N. Nam, T. L. Bui, S. J. Son, S.-W. Joo, *Adv. Funct. Mater.*, **2019**, 1809146.

[30] D. Yang, H. Cho, S. Koo, S. R. Vaidyanathan, K. Woo, Y. Yoon, H. Choo, *ACS Appl. Mater. Interfaces*, **2017**, *9*, 19092.

[31] B.-B. Xu, Y.-L. Zhang, W.-Y. Zhang, X.-Q. Liu, J.-N. Wang, X.-L. Zhang, D.-D. Zhang, H.-B. Jiang, R. Zhang, H.-B. Sun, *Adv. Opt. Mater.*, **2013**, *1*, 56.

[32] K. Wu, T. Li, M. S. Schmidt, T. Rindzevicius, A. Boisen, S. Ndoni, *Adv. Funct. Mater.*, **2018**, *28*, 1704818.

[33] Y. Chen, K. J. Si, D. Sikdar, Y. Tang, M. Premaratne, W. Cheng, *Adv. Opt. Mater.*, **2015**, *3*, 919.

[34] K. J. Si, P. Guo, Q. Shi, W. Cheng, *Anal. Chem.*, **2015**, *87*, 5263.

[35] S.-G. Park, C. Mun, X. Xiao, A. Braun, S. Kim, V. Giannini, S. A. Maier, D.-H. Kim, *Adv. Funct. Mater.*, **2017**, *27*, 1703376.

[36] B. Liu, X. Yao, S. Chen, H. Lin, Z. Yang, S. Liu, .B. Ren, *Adv. Funct. Mater.*, **2018**, *28*, 1802263.

[37] A. Reyer, A. Prinz, S. Giancristofaro, J. Schneider, D. B. Menezes, G. Zickler, G. R. Bourret, M. E. Musso, *ACS Appl. Mater. Interfaces*, **2017**, *9*, 25445.

[38] L.-L. Qu, D.-W. Li, J.-Q. Xue, W.-L. Zhai, J. S. Fossey, Y.-T. Long, *Lab Chip*, **2012**, *12*, 876.

[39] M. Viehrig, A. H. Thilsted, M. Matteucci, K. Wu, D. Catak, M. S. Schmidt, K. Zór, A. Boisen, *ACS Appl. Mater. Interfaces*, **2018**, *10*, 37417.

[40] W. Yan, L. Yang, J. Chen, Y. Wu, P. Wang, Z. Li, *Adv. Mater.*, **2017**, *29*, 1702893.

[41] B. Yan, K. Sun, K. Chao, N. S. Alharbi, J. Li, Q. Huang, *Food Anal. Methods*, **2018**, *11*, 2329.

[42] L.-B. Zhong, J. Yin, Y.-M. Zheng, Q. Liu, X.-X. Cheng, F.-H. Luo, *Anal. Chem.*, **2014**, *86*, 6262.

[43] X. Liu, J. Wang, J. Wang, L. Tang, Y. Ying, *Anal. Chem.*, **2016**, *88*, 6166.

[44] W. Wu, L. Liu, Z. Dai, J. Liu, S. Yang, L. Zhou, X. Xiao, C. Jiang, V. A. Roy, *Sci. Rep.*, **2015**, *5*, 10208.

[45] S. Hu, B.-J. Liu, J.-M. Feng, C. Zong, K.-Q. Lin, X. Wang, D.-Y. Wu, B. Ren, *J. Am. Chem. Soc.*, **2018**, *140*, 13680.

[46] H. H. Richardson, M. T. Carlson, P. J. Tandler, P. Hernandez, A. O. Govorov, *Nano Lett.*, **2009**, *9*, 1139.

[47] B. Demirel, A. Yaras, H. Elcicek, *BAÜ Fen Bil. Enst. Dergisi Cilt*, **2011**, *13*, 26.

[48] TOPAS Advanced Polymers GmbH, Technical Data Sheet, https://topas.com/sites/default/files/TDS_5013L-10_e_US.pdf, accessed: December, 2018.

[49] H. Teng, K. Koike, D. Zhou, Z. Satoh, Y. Koike, Y. Okamoto, *J. Polym. Sci., Part A: Polym. Chem.*, **2009**, *47*, 315.

[50] J. Rieger, *J. Therm. Anal.*, **1996**, *46*, 965.

[51] J. Yang, M. Palla, F. G. Bosco, T. Rindzevicius, T. S. Alstrøm, M. S. Schmidt, A. Boisen, J. Ju, Q. Lin, *ACS Nano*, **2013**, *7*, 5350.

[52] X. Wang, S.-G. Park, J. Ko, X. Xiao, V. Giannini, S. A. Maier, D.-H. Kim, J. Choo, *Small*, **2018**, *14*, 1801623.

[53] R. Feng, R. J. Farris, *J. Micromech. Microeng.*, **2003**, *13*, 80.

[54] K. Du, I. Wathuthanthri, Y. Liu, Y. T. Kang, C.-H. Choi, *Nanotechnology*, **2014**, *25*, 165301.

[55] H. Mao, Y. Zhang, W. Wu, C. Xue, *5th IEEE International Conference on Nano/Micro Engineered and Molecular Systems*, **2010**, 993.

[56] A. Singh, J. Jayaram, M. Madou, S. Akbar, *J. Electrochem. Soc.*, **2002**, *149*, E78.

[57] O. Durucan, K. Wu, M. Viehrig, T. Rindzevicius, A. Boisen, *ACS Sens.*, **2018**, *3*, 2492.

[58] K. Rasmussen, S. Keller, F. Jensen, A. Jorgensen, O. Hansen, *Microelectron. Eng.*, **2013**, *112*, 35.

[59] K. Wu, T. Rindzevicius, M. S. Schmidt, A. H. Thilsted, A. Boisen, *J. Raman Spectrosc.*, **2017**, *48*, 1808.

[60] M. Moskovits, *Phys. Chem. Chem. Phys.*, **2013**, *15*, 5301.

[61] S. T. Chien, *Waveguide fabrication using proton beam writing, Ph.D. Thesis*, National University of Singapore, **2004**.

[62] N. Pazos-Perez, C. S. Wagner, J. M. Romo-Herrera, L. M. Liz-Marzán, F. J. García de Abajo, A. Wittemann, A. Fery, R. A. Alvarez-Puebla, *Angew. Chem. Int. Ed.*, **2012**, *51*, 12688.

[63] K. Wu, T. Rindzevicius, M. S. Schmidt, K. B. Mogensen, A. Hakonen, A. Boisen, *J. Phys. Chem. C*, **2015**, *119*, 2053.

[64] A. H. Thilsted, J. Y. Pan, K. Wu, K. Zor, T. Rindzevicius, M. S. Schmidt, A. Boisen, *Small*, **2016**, *12*, 6745.

[65] P. B. Johnson, R. W. Christy, *Phys. Rev. B*, **1972**, *6*, 4370.

[66] B. H. Ong, X. C. Yuan, S. C. Tjin, *Appl. Opt.*, **2006**, *45*, 8036.

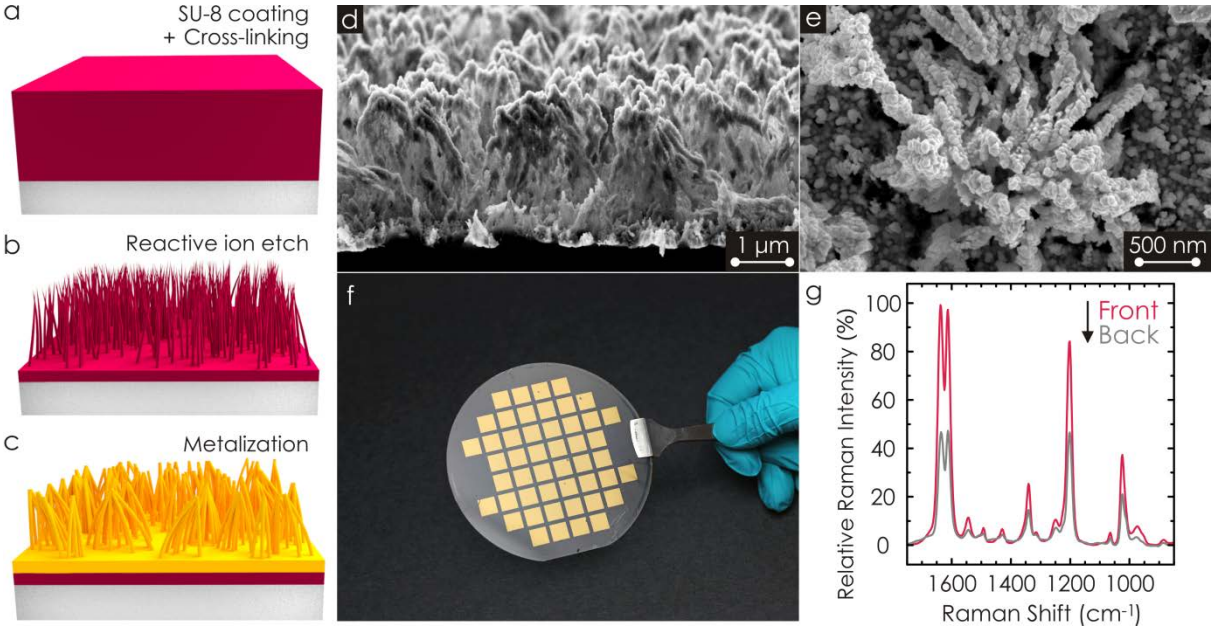

Figure 1. a-c) Schematic of the nanofabrication process of WTNC SERS substrates. d) A cross-sectional SEM image, and e) a top-view SEM image, of a WTNC substrate, produced by 300 s RIE of highly cross-linked SU-8 2035 followed by e-beam evaporation of 200 nm thick gold. f) A photograph of a 4-inch WTNC SERS substrate, taken from its backside. The grid is ascribed to the use of a shadow mask during e-beam evaporation of gold, leaving room for subsequent processes such as dicing to obtain SERS chips and microfluidic integration. g) Two SERS spectra of BPE, obtained respectively from the front and the backside of a WTNC substrate produced with optimal parameters, averaged over the same area containing 25 points.

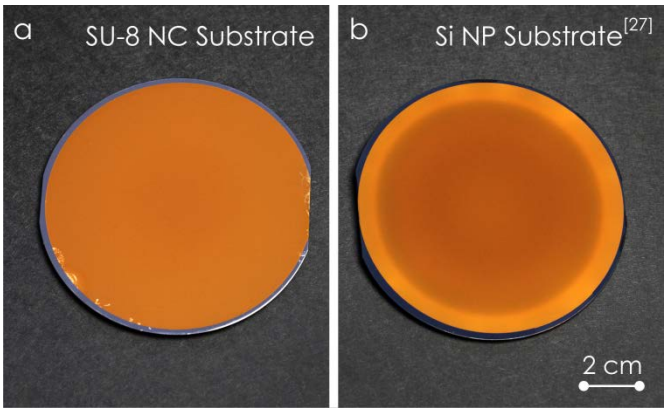

Figure 2. a-b) A nanocoral polymer SERS substrate and a gold capped silicon nanopillar substrate (4-inch), fabricated respectively by maskless O_2 and O_2 + SF_6 RIE, followed by e-beam evaporation of 240 nm gold. Silicon wafers are used for both substrates. The red colors are plasmonic structural colors. The uniform color of the nanocoral substrate indicates excellent uniformity of nanostructures over the wafer. The different colors of the nanopillar substrate with ring patterns indicate structural inhomogeneity across the wafer, caused by macroloading effect during RIE. This leads to poor yield and inconsistent SERS performance across the wafer.[59]

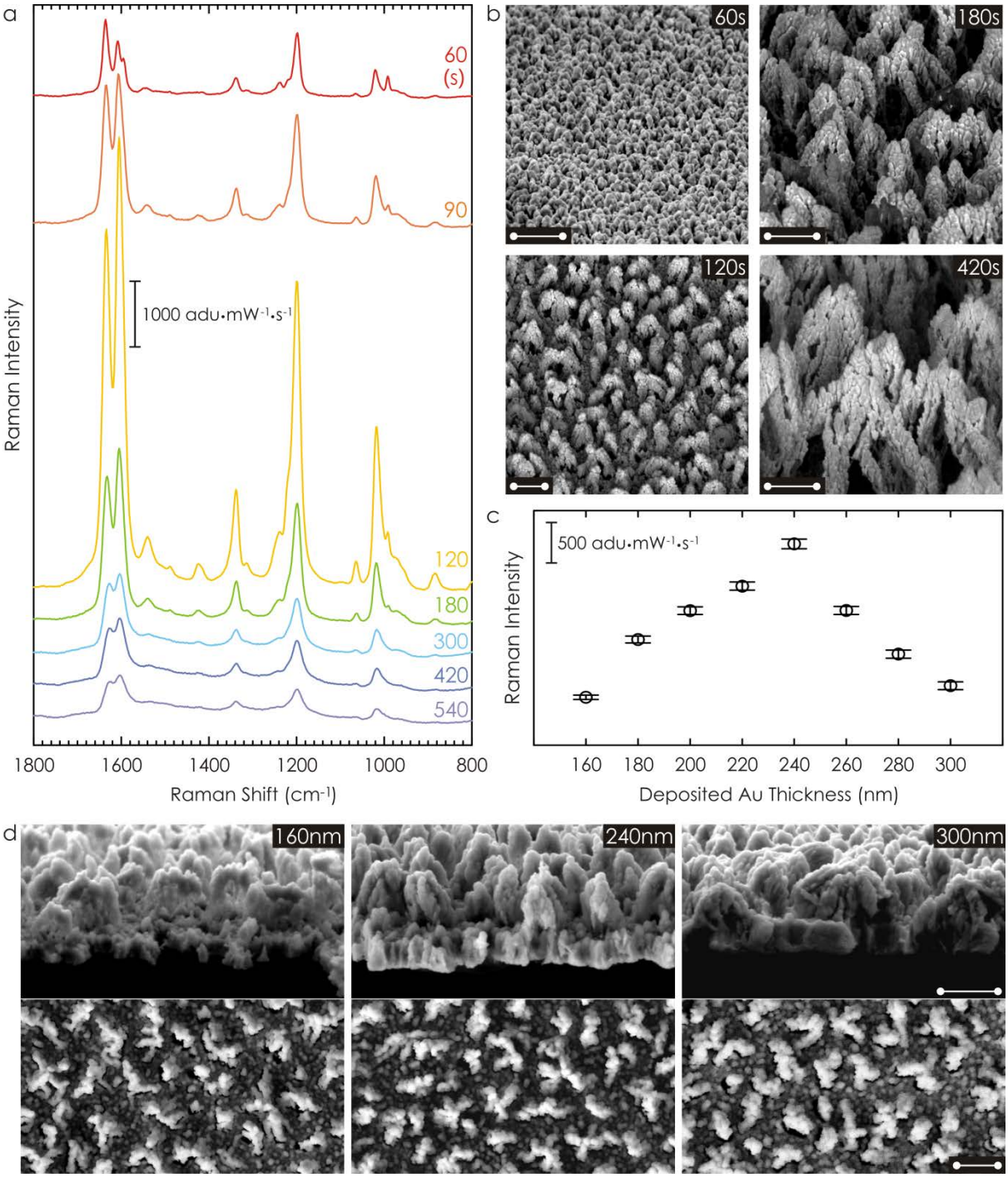

Figure 3. a) Averaged SERS spectra of BPE over 25 locations, obtained on the WTNC substrates produced with different t_{RIE} from 60 - 540 s on SU-8 2035. D_{au} = 200 nm. b) SEM images of samples to be used for a), obtained at a tilt angle of 45°. c) I_{SERS} at the 1200 cm^{-1} Raman band of BPE obtained on WTNC substrates with different D_{au}. The statistical sampling size was 25 for each point. t_{RIE} = 120 s. d) Cross-sectional (first row) and top-view (second row) SEM images of the substrates used for c). a,c) 1 nanomol BPE in 1 µL ethanol solution was pipetted onto each sample. SERS measurement was performed after drying of analyte solution, which took about 5 s. Each SERS spectrum was contributed by ~170 attomol BPE analytes in average. All spectra were collected from the nanostructured surface of the sample near the droplet center. Scale bars: 500 nm.

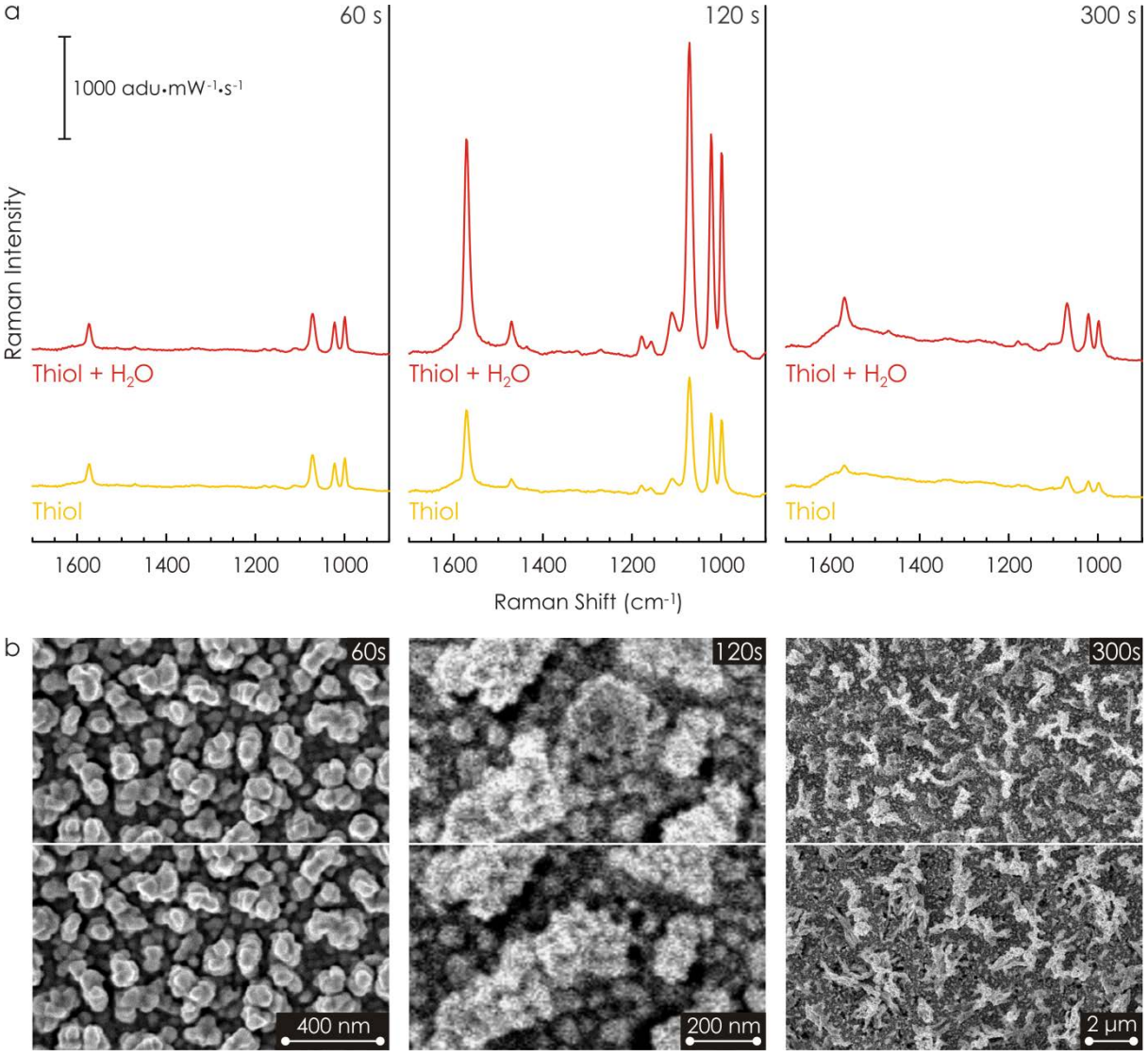

Figure 4. a) Averaged SERS spectra over 25 locations of 1×10^{-3} M thiophenol evaporated for 30 s onto the WTNC substrates, obtained before and after subsequent deposition and evaporation of deionized water on the substrates. The substrates were produced with different t_{RIE} = 60, 120 and 300 s, and the same D_{au} = 200 nm. b) Top-view SEM images of the substrates used for a). Images in the first and second row represent substrates before and after treatment by deposition and evaporation of deionized water, respectively. The images in the first and second rows show the same area for substrates produced with t_{RIE} = 60 and 120 s.

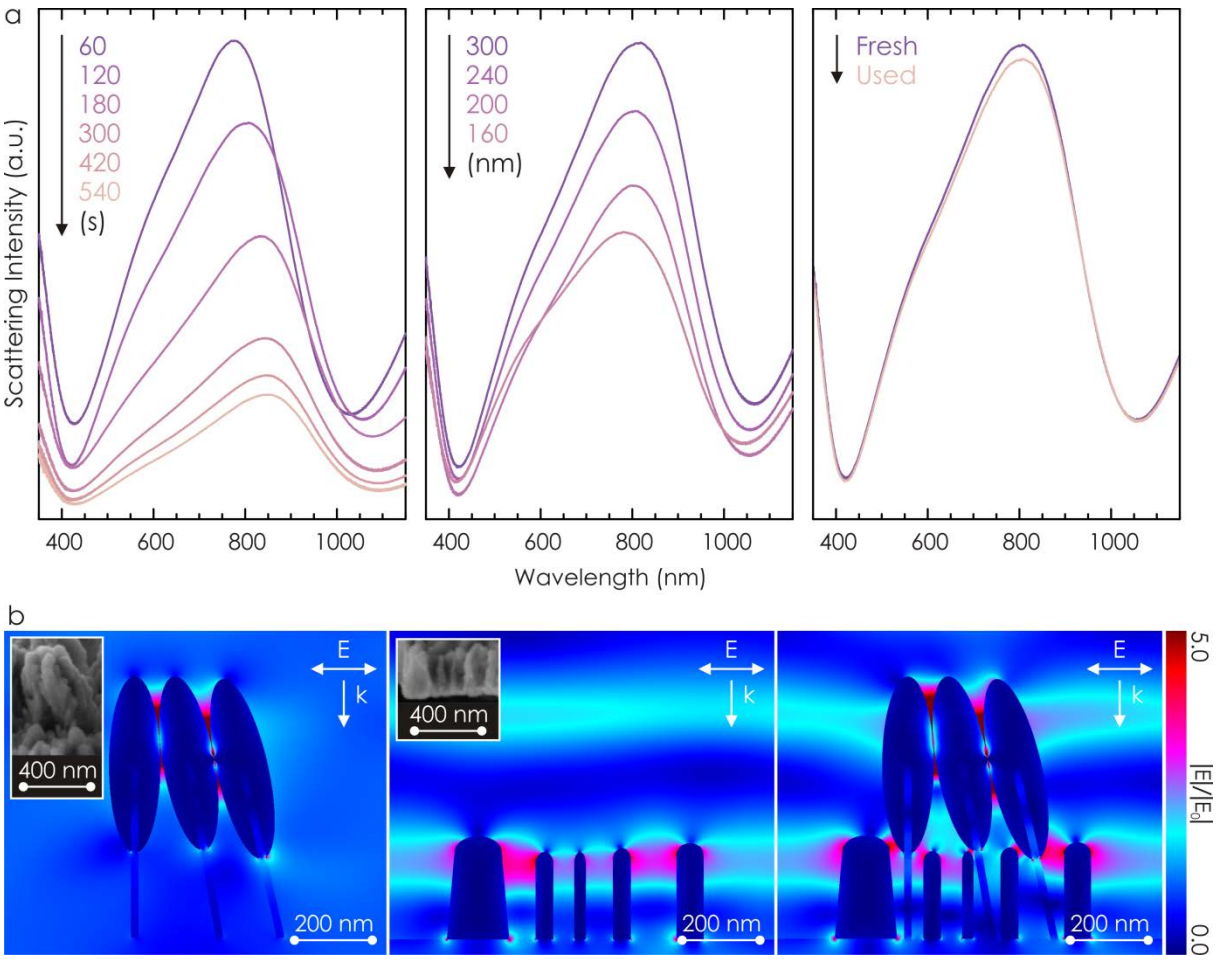

Figure 5. a) Left and middle: dark-field scattering spectra of the WTNC SERS substrates fabricated with different process parameters, measured from the nanostructured sides. Left: D_{au} = 200 nm, t_{RIE} is varied. Middle: t_{RIE} = 120 s, D_{au} is varied. Right: dark-field scattering spectra of a WTNC SERS substrate produced with optimal parameters: t_{RIE} = 120 s and D_{au} = 240 nm, obtained before and after use for detecting analytes in liquid. b) Simulated electrical field enhancement distributions. The structures were modeled according to the inset SEM images, and to the upper middle SEM image in Figure 3d, corresponding to the substrate that produces maximum SERS signals at 780 nm excitation. In the model, the minimum nanogap distance is 1.5 nm. A maximum electrical field enhancement of > 1000 was obtained.

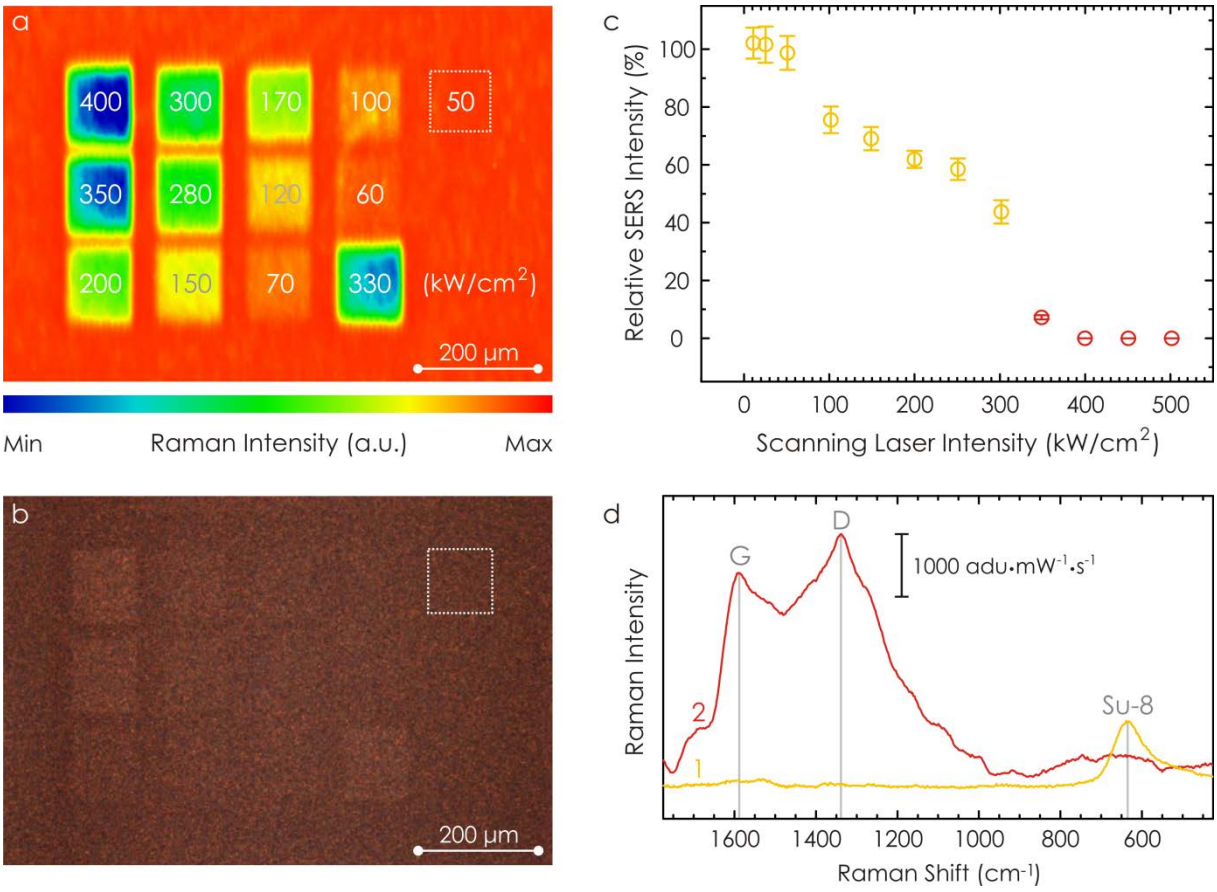

Figure 6. a) SERS image of BPE obtained on the WTNC substrate plotted for the 1200 cm^{-1} Raman band. Before introducing BPE onto the substrate, laser scans were performed on the substrate over 13 square areas, each with the size of 100 × 100 μm^2. Different laser intensity I_{SC} was used for each scan over each square area. Afterwards, 1 nanomol BPE in 1 μL ethanol solution was pipetted onto the substrate. Following the drying of the substrate, the SERS image was obtained under laser intensity of 50 kW cm^{-2}. b) A microscopic image showing the SERS imaged area of Figure 6a. c) Relative I_{SERS} of BPE at 1200 cm^{-1} versus I_{SC}. The experimental procedure was the same as it was in a). 25 spectra near the center of the laser scanning square were used to calculate the average value and the RSD, n = 3. d) Raman spectra obtained on the WTNC substrate after laser scanning, using I_{SC} = 100 kW cm^{-2} (spectrum 1) and 400 kW cm^{-2} (spectrum 2). The absence of the SU-8 band and the appearance of the D- and G- bands of carbon on spectrum 2 indicate pyrolysis of the SU-8. For the SERS images, a step size of 2 μm was used. All signals were obtained from the nanostructured side of the WTNC substrates.

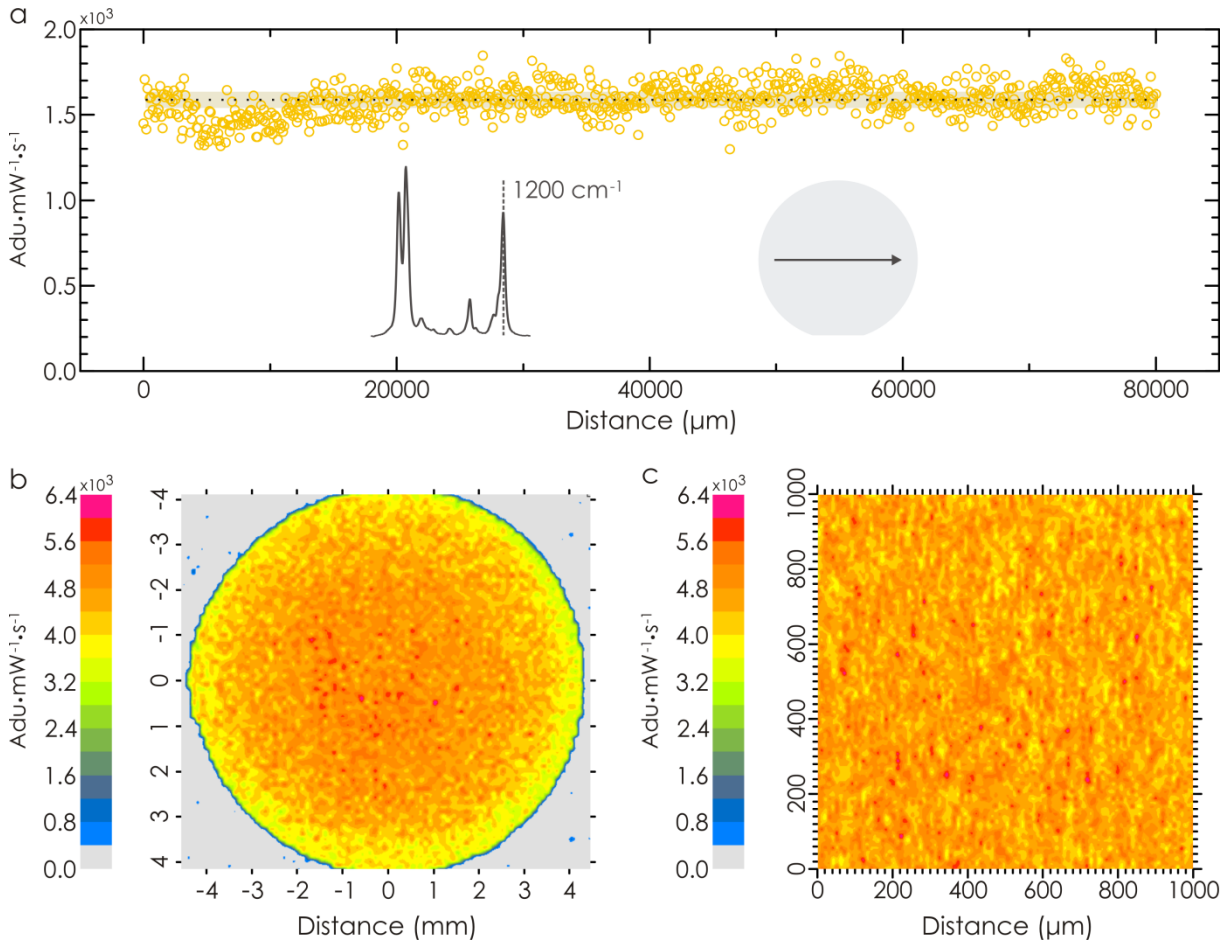

Figure 7. a) SERS line scan of BPE across a 4-inch WTNC wafer plotted at the 1200 cm^{-1} Raman band of BPE. The substrate was incubated in 10^{-4} M BPE in ethanol solution for ~5 seconds and was subsequently dried in air. The distance of the scan was 80 mm, which was the maximum distance allowed by the stage. A step size of 100 μm was used. The shadow region and the dotted line correspond to the RSD and the average intensity, respectively. b) SERS image of BPE at its 1200 cm^{-1} Raman band obtained on the WTNC substrate. 1 nanomol BPE in 1 μL ethanol solution was pipetted onto the substrate. The wet region was quasi-circular with ~4.5 mm in radius. Assuming uniform adsorption of BPE onto the substrate (the radius of the laser spot was 0.94 μm), ~44 attomol BPE in average were probed when obtaining each SERS spectrum. A step size of 100 μm was used. c) SERS image of BPE at its 1200 cm^{-1} Raman band obtained near the center of the droplet area in b). A step size of 10 μm was used. All the signals were obtained from the nanostructured side of the substrates. The applied SERS laser intensity was 50 kW cm^{-2}.

A method to obtain transparent polymer-based SERS substrates with 3D hotspots exhibiting excellent nanoplasmonic heat resistance, ultrahigh SERS sensitivity, and supreme SERS signal uniformity is presented. ~44 attomol BPE is detectable, under very high SERS excitation intensity of 50 kW cm^{-2} within tens of milliseconds. Taking a SERS image containing 10201 of these spectra requires < 5 minutes.

Heat-resistant Polymer SERS Substrates

Kaiyu Wu, Long Quang Nguyen*, Tomas Rindzevicius, Stephan Sylvest Keller and Anja Boisen*

Wafer-scale Polymer-based Transparent Nanocorals with Excellent Nanoplasmonic Photothermal Stability for High-power and Superfast SERS Imaging

ToC figure

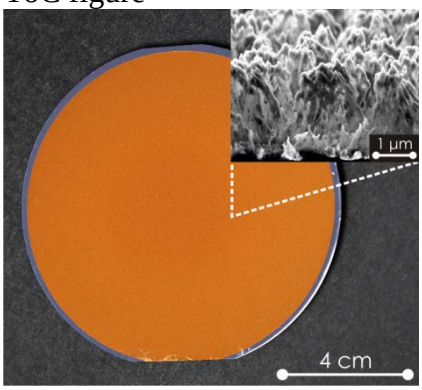

Copyright WILEY-VCH Verlag GmbH & Co. KGaA, 69469 Weinheim, Germany, 2018.

Supporting Information

Wafer-scale Polymer-based Transparent Nanocorals with Excellent Nanoplasmonic Photothermal Stability for High-power and Superfast SERS Imaging

Kaiyu Wu, Long Quang Nguyen*, Tomas Rindzevicius, Stephan Sylvest Keller and Anja Boisen*

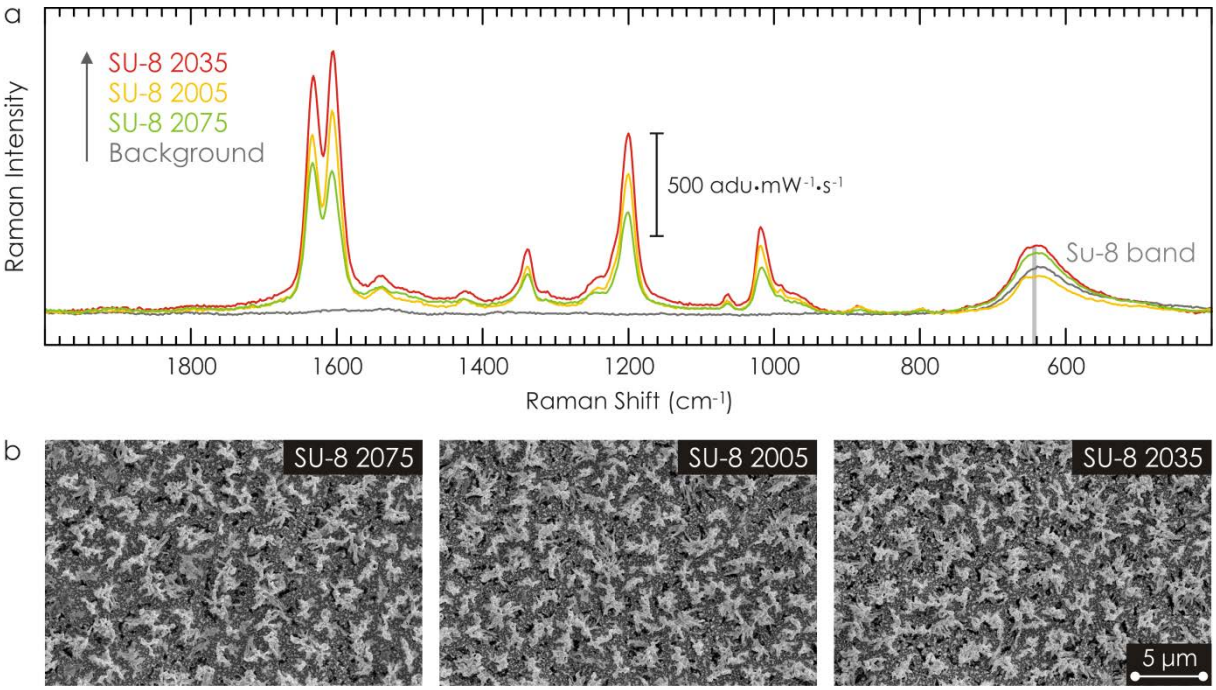

Figure S1. a) Averaged SERS spectra of BPE and averaged SERS background over 25 locations, obtained on WTNC SERS substrates produced with different types of SU-8. The sample for obtaining the background was produced using SU-8 2035. For all the samples, t_{RIE} = 300 s, D_{au} = 200 nm. b) Vertical SEM images of samples used in a). For a), 1 nanomol BPE in 1 µL ethanol solution was pipetted onto each sample. SERS measurement was performed after drying of analyte solution, which took about 5 s. Each SERS spectrum was contributed by ~170 attomol BPE analytes in average. All spectra were collected from the nanostructured surface of the sample near the droplet center.

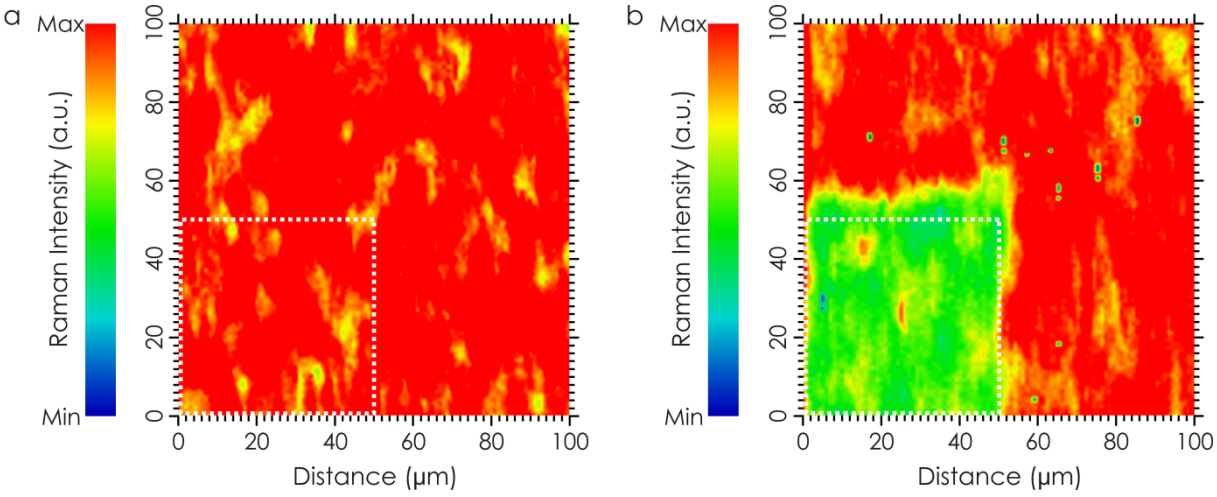

Figure S2. SERS images of BPE obtained on the a) WTNC substrate and b) nanostructured TOPAS-based SERS substrate[39] with similar surface-averaged EFs ~1 × 10^6, plotted at the 1200 cm^{-1} Raman band. Before introducing BPE onto the substrates, laser scans were performed on each substrate over the dotted squares, using a 780 nm laser at 50 kW cm^{-2} and 15 kW cm^{-2} for the WTNC and the TOPAS substrate, respectively. 1 nanomol BPE in 1 μL ethanol solution was then pipetted onto each substrate. SERS images were obtained after drying of the substrates from the nanostructured side, using a 780 nm laser with intensity of 50 kW cm^{-2} and 10 kW cm^{-2}, for a) and b) respectively. To keep the same optical dose, the collection time of each spectrum was 25 ms and 125 ms, for a) and b), respectively. Step size of 1 μm was used. For clarity, the Raman intensity scales were normalized.